Frequency-spectra Impedance Margin Ratio based Stability Analysis of IBR-Penetrated Systems

Ruiting Xu, *Student Member*, *IEEE*, Qin Jiang, *Member*, *IEEE*, Baohong Li, *Member*, *IEEE*, Yikui Liu, *Member*, *IEEE*, Yue Zhu, *Member*, *IEEE*, Yunjie Gu, *Senior Member*, *IEEE*, Tianqi Liu, *Senior Member*, *IEEE*

***Abstract*—The impedance margin ratio (IMR) has been proposed for a global view of the stability margin in the power system with high penetration of inverter-based resources (IBRs). However, the IMR defined at the oscillatory mode can't be intuitively identified from the impedance spectra, increasing the complexity of the stability analysis and losing the physical interpretation. This paper proposes a proportional chain rule among the impedance, the determinant and the oscillatory mode, which provides the guidance of the stability improvement. Then, the frequency-spectra impedance margin ratio (fIMR) is proposed to assess the stability margin at each point of interconnection (POI). All the analysis is based on the impedance's frequency spectra without requirement of the pole identification. Compared with the Nyquist stability criterion, the fIMR provides a unified metric for the stability margin evaluation of all POIs. The proposed fIMR method is verified in a modified 68-bus system and successfully reveals the weak points and guides the impedance reshaping of the apparatus.**

***Index Terms*— small-signal system strength, impedance margin ratio, impedance model, stability analysis, impedance sensitivity.**

I. Introduction

With the soaring penetration of inverter-based resources (IBRs), power system faces increasingly growing risk of oscillation due to their complicated dynamic characteristics, which could cause equipment damage or even power outages [1]-[3]. Stability analysis is vital for revealing the mechanism of oscillations and thereby developing targeted suppression manners.

Stability analysis can be generally conducted based on state space methods and impedance-based methods. The latter is widely applied in stability analyzing of IBR-penetrated systems, due to its remarkable modeling flexibility and advantage of avoiding knowing detailed internal structures of converters [4]-[7]. The impedance model of an IBR can be built based on either analytical derivations or measured impedance data, which also differs the model in the way of being applied in stability analysis.

With a system-level analytical impedance model, where the impedance is analytically expressed with respect to complex frequency "*s*", stability analysis can be conducted with either the nodal-loop model [8]-[10] or the whole-system model based methods [11]. When being applied to a certain oscillatory mode obtained from the analytical model, both the nodal-loop model based modal impedance analysis and the whole-system model-based mode-impedance participation analysis could reveal the root cause of oscillation and thereby provide guidance for oscillation suppressing [12].

The participation factor in the nodal-loop model is unable to indicate the direction on which tuning the parameter will damp the oscillatory mode. By contrast, the whole-system model could show that the mode-impedance participation factor is indeed the residue of the whole-system admittance at the point of inter-connection (POI) [13], including the direction of damping. Under the framework of the whole-system model, considering the mode-impedance participation factor, impedance margin ratio (IMR) is proposed as a metric of the system's small-signal strength at the POI [14]. IMR measures the stability margin of each POI and helps identify the most critical POI.

The whole-system model, together with IMR, offers a clear and effective means for analyzing the stability of IBR-penetrated systems, and thereby providing thorough guidance for reshaping the IBR impedance at individual oscillatory modes to enhance system stability. However, due to commercial confidentiality, IBR vendors usually merely provide discrete impedance spectra or compiled electromagnetic transient simulation models of their apparatus, which hinders the construction of analytical models and transparent analysis [15].

Classical Nyquist Stability Criterion (NSC) is a frequency-spectra impedance data based stability analysis method that requires no pre-established analytical model [16]-[17], particularly focusing on single-input single-output (SISO) systems. In the system where multiple IBRs have significant participation in oscillation, NSC that originally targets at SISO systems easily produces inconsistent results because of passively neglecting the correlation between the individually obtained results of focused POIs. To this end, generalized Nyquist stability criterion (GNSC), an extension of NSC, is proposed to handle the case of multi-input multi-output (MIMO) systems [18]-[22]. With GNSC, based on eigen-decomposition, the determinant-impedance sensitivity is calculated [23]-[24] in accompanying to reflect the influence of the impedance on stability of the system, with which, this method in fact could reveal the root cause of oscillation, similarly to the nodal-loop model and the whole-system model based analysis.

However, eigen-decomposition requires knowing the values of all elements in the impedance matrices of all the connected apparatus and the network. This significantly reduces the practical applicability of GNSC, as measuring the impedance between two nodes, i.e. acquiring non-diagonal elements in the impedance matrix of the system, that are geographically far apart in the system is difficult. Moreover, unlike the whole system model-based method, with GNSC, its essential process of categorizing every apparatus as sources or loads is

cumbersome especially when facing massive IBRs, and plotted Nyquist curves could be extremely complicated making the judgment of system stability highly challenging. These, indeed, have created obstacles to applying GNSC in large-scale systems.

Indeed, an idea combining merits of analytical model based methods and NSCs is to identify the parameters of the analytical model with measured data. Mode identification methods [25]-[28] transform measured impedance spectra back to analytical models with respect to the Laplace operator "*s*". Then, the whole-system model based stability analysis is able to be performed. However, the identification process loses intuition to physical mechanism as the identified result is the denominator and numerator polynomials having no connection with the original system.

Intuitively, analytical models of IBRs should also be identified, particularly focusing on reshaping their impedance at the oscillatory mode in the next. However, in some cases, the oscillatory mode of interest may correspond to small impedance magnitudes of the apparatus, making the apparatus impedance identification easily vulnerable to the measurement noise [26]. This hinders the following reshaping the impedance at the oscillatory mode.

Therefore, in this paper, impedance-determinant-mode chain rule is firstly proposed, and on this basis a novel stability margin indicator named as frequency-spectra impedance margin ratio (fIMR) is derived. With fIMR, we further propose a stability analyzing method for impedance data based large-scale power systems.

Specially, this method inherits multiple merits of whole-system model based methods, including the ability of analyzing participation level, evaluating stability margin, and guiding the reshaping of the apparatus' impedance. Moreover, fIMR analysis is applied at the imaginary axis instead of the oscillatory mode and no mode identification is required. Compared to GNSC, being more practically applicable, it merely uses local impedance at individual POIs, avoiding acquisition of all elements in related impedance matrices of the entire system.

The paper is organized as follows. The impedance-determinant-mode relationship over the complex plane is fully discussed in Section II, where the impedance participation factor on the frequency spectra is also defined. The fIMR based stability analysis and stability improving strategy are proposed in Section IV. The case study is presented in Section IV, and the conclusions are summarized in Section V.

II. Sensitivity Analyzing of the Impedance, the Determinant and the Mode

System stability analysis with a whole-system model is generally implemented on a known oscillatory mode together with the corresponding residue obtained from the analytical model. Using direct frequency-spectra data, stability analysis is performed at the imaginary axis rather than the mode. The relationship between the impedance and the mode in areas apart from the mode on the complex plane requires careful analysis.

In this section, we review the mode-impedance sensitivity at oscillatory modes and then explain the limitations when the whole-system model being applied in non-mode areas. Then, towards frequency-spectra data based stability analysis, a more general chain rule that depicts the small-signal sensitivity between the impedance, the determinant of the impedance, and the mode is identified.

A. The Mode-impedance Sensitivity at the Oscillatory Mode

The whole system model is well introduced in reference [11], where the whole-system admittance is defined as $\boldsymbol{Y}^{\mathrm{sys}}$ as in (1), which illustrates the dynamic relationship between the injected small voltage perturbance $\tilde{\boldsymbol{v}}$ and the response current $\Delta\boldsymbol{i}$.

$$\Delta\boldsymbol{i}(s)=\boldsymbol{Y}^{\mathrm{sys}}(s)\tilde{\boldsymbol{v}}(s) \tag{1}$$

The inverse matrix of $\boldsymbol{Y}^{\mathrm{sys}}$ is indeed the sum of the apparatus' impedance matrix $\boldsymbol{Z}_{\mathrm{A}}$ and the network impedance matrix $\boldsymbol{Z}_{\mathrm{N}}$, which is denoted as $\boldsymbol{Z}^{\mathrm{sum}}$. This is shown in (2) and (3).

$$\boldsymbol{Z}^{\mathrm{sum}}(s)=\boldsymbol{Y}^{\mathrm{sys}}(s)^{-1} \tag{2}$$

$$\boldsymbol{Z}^{\mathrm{sum}}(s)=\boldsymbol{Z}_{\mathrm{A}}(s)+\boldsymbol{Z}_{\mathrm{N}}(s) \tag{3}$$

Without of loss generality, considering the apparatus at the *k*th point of interconnection (POI-*k*), $\boldsymbol{Z}_k^{\mathrm{sum}}$, $\boldsymbol{Z}_{\mathrm{A}k}$, and $\boldsymbol{Z}_{\mathrm{N}k}$ respectively denote the *k*th diagonal block of $\boldsymbol{Z}^{\mathrm{sum}}$, $\boldsymbol{Z}_{\mathrm{A}}$, and $\boldsymbol{Z}_{\mathrm{N}}$, which are all 2×2 matrices, when the model is built on the d-q frame. With knowing parameters of the apparatus at POI-*k* and the unchanged grid side of the system, considering a small variation in $\boldsymbol{Z}_{\mathrm{A}k}$, the small-signal equation (4) holds.

$$\Delta\boldsymbol{Z}_k^{\mathrm{sum}}(s)=\Delta\boldsymbol{Z}_{\mathrm{A}k}(s)+\Delta\boldsymbol{Z}_{\mathrm{N}k}(s)=\Delta\boldsymbol{Z}_{\mathrm{A}k}(s) \tag{4}$$

As shown in (5), the oscillatory modes of the system correspond to the zeros of the determinant of $\boldsymbol{Z}^{\mathrm{sum}}$, which align with the poles of the determinant of $\boldsymbol{Y}^{\mathrm{sys}}$.

$$\det\left(\boldsymbol{Z}^{\mathrm{sum}}(\lambda)\right)=\det\left(\boldsymbol{Y}^{\mathrm{sys}}(\lambda)\right)^{-1}=0 \tag{5}$$

Performing the first-order Taylor expansion on (5), the mode-impedance relationship can be finally represented as in (6). The detailed derivation process is well discussed in reference [12]. In (6), $\boldsymbol{Y}_{kk}^{\mathrm{sys}}$ is the *k*th diagonal block of $\boldsymbol{Y}^{\mathrm{sys}}$; $\mathrm{Res}_\lambda\boldsymbol{Y}_{kk}^{\mathrm{sys}}$ is the residue matrix of $\boldsymbol{Y}_{kk}^{\mathrm{sys}}$ at the mode λ; and superscript * means the conjugate transpose of the matrix.

$$\Delta\lambda=\left\langle-\mathrm{Res}_\lambda^{*}\boldsymbol{Y}_{kk}^{\mathrm{sys}},\Delta\boldsymbol{Z}_{\mathrm{A}k}(\lambda)\right\rangle \tag{6}$$

From (6) that depicts the mode changing with the influence of impedance, it can be found that the residue of the whole-system admittance is, in fact, equal to the mode-impedance sensitivity. Based on this, it can be concluded that the impedance reshaping direction of apparatus that improves stability is identical to the direction of the residue. In addition, the magnitude of the residue reflects the participation level of the impedance on a certain oscillatory mode λ. It can be seen, for a certain mode λ, mode-impedance analysis becomes effective with equation (6).

The residue-based property exhibited by (6) can be further utilized for estimating small-signal strength of the system. According to the impedance margin ratio (IMR) theory proposed in [14], as shown in (7), the magnitude of impedance sensitivity depicts the small-signal stability margin at POI-*k* of the system. In (7), $\|\cdot\|$ denotes the Frobenius norm of a matrix

and $||\Delta Z_{Ak}(\lambda)||_{\max}$ represents the maximum allowed variation of the apparatus' impedance at the mode λ.

$$\mathrm{IMR}=\frac{\left\|\Delta Z_{\mathrm{A}k}(\lambda)\right\|_{\max}}{\left\|Z_{\mathrm{A}k}(\lambda)\right\|}=\frac{|\sigma_{\mathrm{c}}|}{\left\|R_{kk}\right\|\left\|Z_{\mathrm{A}k}(\lambda)\right\|} \tag{7}$$

It is worthwhile to emphasize that equations (6) and (7) hold at $s=\lambda$, as they are derived based on the Tylor expansion of (5) at the mode λ, while the expansion prerequisite positions and residues of the modes that can be calculated from the analytical model of the entire system. However, as aforementioned, commercial confidence hinders the construction of the analytical model, which strongly compromises the practical application of equation (6).

Indeed, instead of reconstructing the analytical model from the frequency-spectra data, directly analyzing these frequency-spectra data on the imaginary axis could avoid inaccuracy in mode identification. To this end, a general analytical model-free mode-impedance sensitivity analyzing method on the entire complex plane becomes appealing.

B. The Chain Rule of Impedance-determinant-mode Sensitivity

The derivative of the determinant Z_{det} with respect to the element of $\boldsymbol{Z}^{\mathrm{sum}}$ gives the cofactor matrix of $\boldsymbol{Z}^{\mathrm{sum}}$, as shown in (8), where $\boldsymbol{F}$ is the cofactor matrix of $\boldsymbol{Z}^{\mathrm{sum}}$. The subscripts h and l represent h-th row and l-th column of the matrix.

$$\frac{\partial Z_{\mathrm{det}}}{\partial Z_{hl}^{\mathrm{sum}}}(s)=F_{hl}(s) \tag{8}$$

According to (8), the variance of the determinant Z_{det} can be expressed with the Frobenius inner product as shown in (9), where $^-$ represents the complex conjugate of the matrix.

$$\Delta Z_{\mathrm{det}}(s)=\left\langle \bar{\boldsymbol{F}}(s),\Delta \boldsymbol{Z}^{\mathrm{sum}}(s)\right\rangle \tag{9}$$

Then, (10) holds, as the whole-system admittance $\boldsymbol{Y}^{\mathrm{sys}}$ is the inverse matrix of the impedance matrix $\boldsymbol{Z}^{\mathrm{sum}}$.

$$\boldsymbol{Y}^{\mathrm{sys}}(s)=\frac{\boldsymbol{F}(s)}{Z_{\mathrm{det}}(s)} \tag{10}$$

According to (4), $\Delta \boldsymbol{Z}_k^{\mathrm{sum}}$ is equal to $\Delta \boldsymbol{Z}_{\mathrm{A}k}$ considering the impedances of the network and other apparatus all remain unchanged. Then, substituting (10) into (9) yields (11).

$$\frac{\Delta Z_{\mathrm{det}}(s)}{Z_{\mathrm{det}}(s)}=\left\langle \bar{\boldsymbol{Y}}_{kk}^{\mathrm{sys}}(s),\Delta \boldsymbol{Z}_{\mathrm{A}k}(s)\right\rangle \tag{11}$$

Equation (11) establishes the small-signal sensitivity of the impedance matrix of apparatus over the determinant of the nodal impedance matrix, where the coefficient is the whole-system admittance. Moreover, from the whole-system admittance in (1), the whole-system admittance represents the proportion between the excited current and the excitation voltage source. Therefore, the impedance participation factor can reflect the magnitude of the oscillation observed at the focused POI. Thus, as in (12), we define the whole-system admittance as the participation factor.

$$\mathbf{PF}_k(s)\triangleq \boldsymbol{Y}_{kk}^{\mathrm{sys}}(s) \tag{12}$$

When focusing on the variation of one single element of $\Delta \boldsymbol{Z}_{\mathrm{A}k}$, i.e., $\Delta Z_{\mathrm{A}k}$, the following observations can be made from equation (11):

i) When the impedance $Z_{\mathrm{A}k}$ changes along the direction of the inverse of Y_{kk}^{sys}, the determinant Z_{det} also changes along the direction from the origin to Z_{det} on the complex plane.

ii) $\left|\Delta Z_{\mathrm{A}k}\right|/\left|Y_{kk}^{\mathrm{sys}-1}\right|$ and $|\Delta Z_{\mathrm{det}}|/|Z_{\mathrm{det}}|$ are equal.

Comparing with equation (6), which is linearized at the oscillatory mode λ, the frequency of equation (11), namely s, can be arbitrary. Therefore, the impedance-determinant sensitivity has a broader valid area on the complex plane.

The Frobenius inner product of $\boldsymbol{Y}_{kk}^{\mathrm{sys}}$ and $\boldsymbol{Z}_{\mathrm{A}k}$ further illustrates the entire apparatus' own influence on the determinant. Considering a small change of $\boldsymbol{Z}_{\mathrm{A}k}$ aligned to its original direction is introduced, the change of the determinant could reflect the influence of the apparatus on the stability. To calculate that, assuming the perturbation of the apparatus impedance $\Delta \boldsymbol{Z}_{\mathrm{A}k}$ is aligned to its original impedance $\boldsymbol{Z}_{\mathrm{A}k}$, i.e., $\Delta \boldsymbol{Z}_{\mathrm{A}k}=\varepsilon \boldsymbol{Z}_{\mathrm{A}k}$, the according change in the determinant can be calculated as in (13), where ε is a small positive real number.

$$\mathrm{CF}_k(s)=\frac{\Delta Z_{\mathrm{det}}(s)}{Z_{\mathrm{det}}(s)}=\varepsilon\left\langle \bar{\boldsymbol{Y}}_{kk}^{\mathrm{sys}}(s),\boldsymbol{Z}_{\mathrm{A}k}(s)\right\rangle \tag{13}$$

We take CF_k as the contribution factor as it describes the contribution of the impedance of the apparatus to the determinant of the system. For comparing the contributions of different apparatus, real and imaginary parts of the contribution factors are both normalized.

For further analyzing the influence of the impedance to the system stability, the determinant-mode sensitivity is studied. Given a focused mode, e.g., $\lambda_{\mathrm{c}}=\sigma_{\mathrm{c}}+j\omega_{\mathrm{c}}$, the determinant Z_{det} can be decomposed into (14), where G represents the rest part of Z_{det}.

$$Z_{\mathrm{det}}(s)=(s-\lambda_{\mathrm{c}})G(s) \tag{14}$$

Applying the first-order Tylor expansion on (14), (15) can be obtained. From (15), the contribution of $\Delta\lambda_{\mathrm{c}}$ and ΔG to ΔZ_{det} is associated with $(s-\lambda_{\mathrm{c}})$ and $G(s)$.

$$\Delta Z_{\mathrm{det}}(s)=(s-\lambda_{\mathrm{c}})\Delta G(s)-G(s)\Delta\lambda_{\mathrm{c}} \tag{15}$$

As in (16), when the studied frequency, namely s, is close to λ_{c}, i.e., the absolute value of $(s-\lambda_{\mathrm{c}})$ is much smaller than that of $G(s)$, the perturbation of Z_{det} can be approximated merely with $\Delta\lambda_{\mathrm{c}}$, as shown in (17).

$$\left|(s-\lambda_{\mathrm{c}})\Delta G(s)\right|\ll\left|G(s)\Delta\lambda_{\mathrm{c}}\right| \tag{16}$$

$$\frac{\Delta Z_{\mathrm{det}}(s)}{Z_{\mathrm{det}}(s)}\simeq-\frac{G(s)}{Z_{\mathrm{det}}(s)}\Delta\lambda_{\mathrm{c}}=\frac{\Delta\lambda_{\mathrm{c}}}{\lambda_{\mathrm{c}}-s} \tag{17}$$

Equation (17) implies the following:

i) When the determinant Z_{det} increases along the direction from the origin, the mode λ_{c} changes from the frequency s to λ_{c} on the complex plane.

ii) $|\Delta Z_{\mathrm{det}}|/|Z_{\mathrm{det}}|$ and $|\Delta\lambda_{\mathrm{c}}|/|s-\lambda_{\mathrm{c}}|$ are equal.

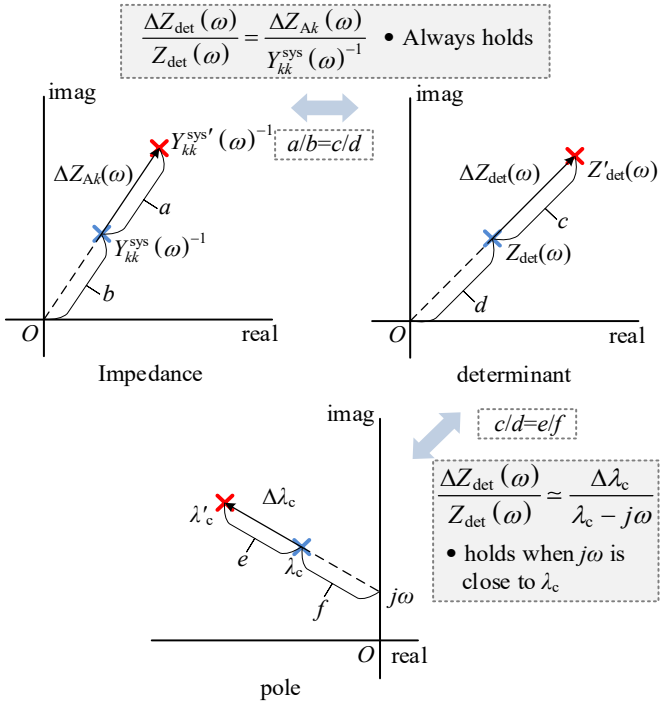

Fig. 1. Illustration of the impedance-determinant-mode relationship.

As an example, with frequency-spectra data, by substituting frequency s with $s=j\omega$, the meanings of (11) and (17) can be illustrated in Fig. 1. In Fig. 1, the apparatus' impedance is plotted in the scalar form for convenience. Variations happen on the impedance, the determinant, and the mode simultaneously. As the inverse of the whole system admittance, namely $Y_{kk}^{sys}(\omega)^{-1}$, moves away from the origin, the determinant $Z_{\det}(\omega)$ moves away from the origin as well. Then, when the condition (16) is satisfied, mode λ_c moves away from $(0, \omega)$ accordingly. The variation degrees, i.e., the proportions of the variations over the original values, are identical for the impedance, the determinant, and the mode.

It also can be seen from Fig. 1 that when performing the stability analysis with the frequency-spectra data, through revising the impedance Z_{Ak} reversely from the phase of $Y_{kk}^{sys}(\omega)$, mode λ_c will move away from the imaginary axis. When mode λ_c is originally stable, according to (17), λ_c becomes more stable as its real part is negative, while when mode λ_c is unstable, its real part will increase, leading to severer oscillation. If the frequency-spectra data is extracted from a stable system where the real part of the oscillatory mode is negative, revising the impedance Z_{Ak} reversely with $Y_{kk}^{sys}(\omega)$ will improve the stability. Moreover, if the discussed frequency ω equals to the mode frequency ω_c, the efficiency of the impedance reshaping will be maximized, as $\Delta\lambda_c$ will totally be a real number and directly influences the damping of the mode.

In fact, equations (11) and (17) form the impedance-determinant-mode chain rule, which provides an enlightening guidance on impedance based stability analysis. Combining equation (11) and (17) can provide accurate stability analysis result. It is worthwhile to mention that when the oscillatory mode has large real part and the system has large stability margin, the condition of (16) may not be satisfied, and accordingly (17) becomes invalid. However, the necessity of adjusting a mode will also decrease if the mode has a large real part. Moreover, although (17) is not exact and exactness may not be attainable, the principle of driving the determinant away from the origin remains valid, because, according to (5), the determinant consistently approaches the origin before the system turns unstable. Thus, a general guidance of impedance reshaping, i.e., revising Z_{Ak} reversely from the phase of $Y_{kk}^{sys}(\omega)$ as in (11), is still useful.

Generally, improving stability of IBR penetrated systems relies on firstly identifying the influence of parameters and added control strategies to the impedance spectra of an apparatus [29]-[30], namely the impedance-parameter sensitivity. The impedance-parameter sensitivity [12] is referred as in (18).

$$\boldsymbol{S}_{ZAk,\rho}(\omega)=\frac{\partial \boldsymbol{Z}_{Ak}(\omega)}{\partial\rho}\simeq\frac{\boldsymbol{Z}_{Ak,\Delta\rho}(\omega)-\boldsymbol{Z}_{Ak}(\omega)}{\Delta\rho} \tag{18}$$

Substituting (18) into (11), the determinant-parameter sensitivity can be calculated as shown in (19). Under the guidance of (19), the influential parameters can be retuned to move the determinant away from the origin.

$$\begin{aligned} S_{Z\det,\rho}(\omega)&=\frac{|\rho|}{Z_{\det}(\omega)}\frac{\partial Z_{\det}(\omega)}{\partial\rho}\\ &=|\rho|\left\langle \bar{\boldsymbol{Y}}_{kk}^{sys}(\omega),\boldsymbol{S}_{ZAk,\rho}(\omega)\right\rangle \end{aligned} \tag{19}$$

III. The Frequency-Spectra Impedance Margin Ratio

Focusing on the impedance at the oscillatory mode, in reference [14], IMR is proposed for measuring the stability margin approximately from the perspective of impedance reshaping. By contrast, with the more general impedance-determinant-mode chain rule, in this paper, IMR is expanded utilizing the data of frequency response and, on this basis, frequency-spectra impedance margin ratio (fIMR) is defined. Combining the determinant-impedance sensitivity and the proposed fIMR, a frequency-spectra data based stability analysis method is proposed and compared with the Nyquist stability criterion (NSC) and the Generalized stability criterion (GNSC).

A. Definition

Considering the system becomes critically stable after the impedance variation of the apparatus, which is denoted as $\Delta\boldsymbol{Z}_{Ak}$. According to (5), the determinant of the impedance matrix $\boldsymbol{Z}^{sum}(\omega)$ will become zero. This is shown in (20), where the determinant of the loop impedance is represented with $Z_{\det}(\omega)$.

$$Z_{\det}(\omega)+\Delta Z_{\det}(\omega)=0 \tag{20}$$

Assuming an variation with unknown direction of the determinant $Z_{\det}(\omega)$, to prevent $Z_{\det}(\omega)$ from falling to zero, we restrict the variation, denoted as $\Delta Z_{\det}(\omega)$, to be no greater than the absolute value of $Z_{\det}(\omega)$, as shown in (21).

$$\left|\Delta Z_{\det}(\omega)\right|_{\max}=\left|Z_{\det}(\omega)\right| \tag{21}$$

Substituting (11) into (21) and applying Cauchy inequality, we can obtained (22).

$$\left\|\Delta \boldsymbol{Z}_{Ak}(\omega)\right\|_{\max}=\left\|\boldsymbol{Y}_{kk}^{sys}(\omega)\right\|^{-1} \tag{22}$$

Equation (22) indicates that the allowed maximum variation of the apparatus' impedance $\left\|\Delta \boldsymbol{Z}_{Ak}(\omega)\right\|_{\max}$ is equal to the inverse of the whole-system admittance's norm $\left\|\boldsymbol{Y}_{kk}^{sys}(\omega)\right\|$.

The concept of the system's stability margin is illustrated in Fig. 2. The impedance of the apparatus is represented in in scalar form. The dotted circles represent the stability margin of the system. Based on (11), when the impedance of the apparatus $Z_{Ak}(\omega)$ is changed to $Z'_{Ak}(\omega)=Z_{Ak}(\omega)+\Delta Z_{Ak}(\omega)$, the perturbed determinant becomes $Z'_{det}(\omega)=Z_{det}(\omega)+\Delta Z_{det}(\omega)$. When the perturbed determinant $Z'_{det}(\omega)$ decreases to zero, the system becomes critically stable with no stability margin. Thus, the magnitude of the original determinant $|Z_{det}(\omega)|$ is the maximum boundary of $\Delta Z_{det}(\omega)$ as in (21). Then, the boundary of $\Delta Z_{Ak}(\omega)$ can be calculated according to (22).

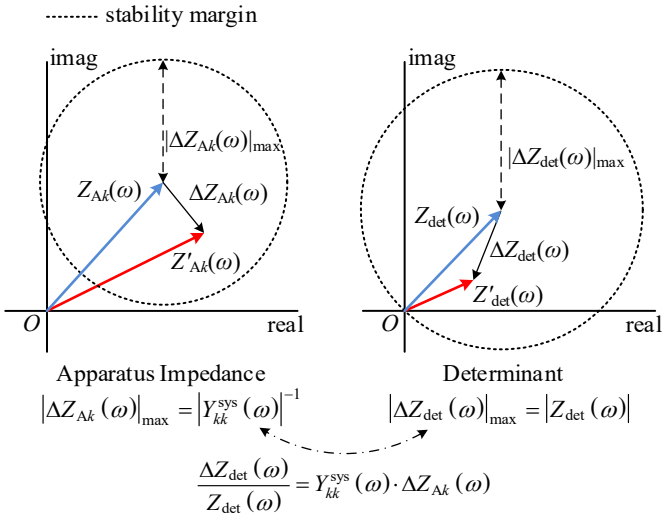

Fig. 2. Illustration of the system's stability margin.

Based on the above analysis, the stability margin of POI-k at the frequency ω can be represented with the relative size of the allowed maximum variation with respect to the norm of the original impedance of the apparatus. Thus, as shown in (23), we novelly redefine IMR at the frequency ω as the proportion of the allowed maximum impedance variation $\left\|\Delta \boldsymbol{Z}_{Ak}(\omega)\right\|_{\max}$ over the norm of the original impedance of the apparatus at the studied frequency $\left\|\Delta \boldsymbol{Z}_{Ak}(\omega)\right\|$. Then, the redefined IMR is named as frequency-spectra impedance margin ratio (fIMR).

$$\text{fIMR}=\frac{\left\|\Delta \boldsymbol{Z}_{Ak}(\omega)\right\|_{\max}}{\left\|\boldsymbol{Z}_{Ak}(\omega)\right\|} \tag{23}$$

Substituting (22) into (23) yields (24), which is the inverse of the product of Frobenius norms of the whole-system admittance and the at apparatus' impedance at POI-k. Equation (24) indicates that fIMRs are distinct as the frequency varies, and are different at different POIs.

$$\text{fIMR}=\frac{1}{\left\|\boldsymbol{Y}_{kk}^{sys}(\omega)\right\|\left\|\boldsymbol{Z}_{Ak}(\omega)\right\|} \tag{24}$$

Therefore, the proposed fIMR is a metric reflecting different POIs' small-signal stability margin at the frequency ω. Large fIMR reflects a stable system. It can be directly calculated using the frequency domain impedance data and intuitively indicates the strength of the system without knowing the values and residues of the modes. In stability analysis, attention is usually attracted by the modes with small real part, whose frequency ω_c is usually observable at the peaks of the whole-system admittance curve. Thus, the fIMR at ω_c should be the focus.

The analysis process of fIMR is illustrated in Fig. 3. The fIMR curve in (24) is plotted using the frequency response data acquired either from an analytical model or measurement. The peaks with different frequencies of the whole-system admittance curves are identified. As the whole-system admittance at all POIs share the same poles, there will be multiple peaks with close frequencies. Then, the fIMR curves are plotted, where we should focus on their value at the modes' frequencies. The system's stability margin becomes the smallest at the bottom of the fIMR curves.

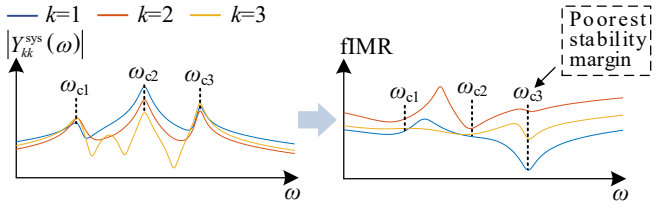

Fig. 3. fIMR based stability analysis.

fIMR reflects the small-signal strength of the system at different POI at the focused frequency. When fIMR is small, a slight variation of the apparatus' impedance may lead to instability, which indicates a poor strength at the POI. Based on the experience of case studies, the guideline of fIMR is suggested as follows:

- fIMR>0.5: The stability margin is sufficient . The system is unlikely to oscillate unless large impedance disturbance happens.
- fIMR<0.5 and fIMR>0.1: The stability margin is barely sufficient. Small change of the impedance at the discussed frequency may lead to instability.
- fIMR<0.1 and fIMR>0: The stability margin is deficient. Oscillation can easily take place even when there is only slight disturbance of the impedance.

Finally, based on the fIMR and the chain rule, the stability margin is approximated and the apparatus' impedance can be reshaped through retuning the parameters. The process of the fIMR based stability analysis method is illustrated in Fig. 4.

i) Frequency response data acquisition: at the focused POIs, acquire the whole system admittance $\boldsymbol{Y}_{kk}^{sys}(\omega)$ and the apparatus' impedance $\boldsymbol{Z}_{Ak}(\omega)$ through online measurement.

ii) Stability analysis: select the peaks of the whole-system admittance curves as the mode frequencies where the participation factor, the contribution factor, and fIMR are calculated. The participation factor and the contribution factor respectively reflect the influence of the impedance element and the entire apparatus on stability. Stability margins at different mode frequencies and POIs are compared using fIMR.

iii) Impedance reshaping: re-tune the parameters of POIs with deficient stability margin and reshape their impedances under the guidance of the chain rule.

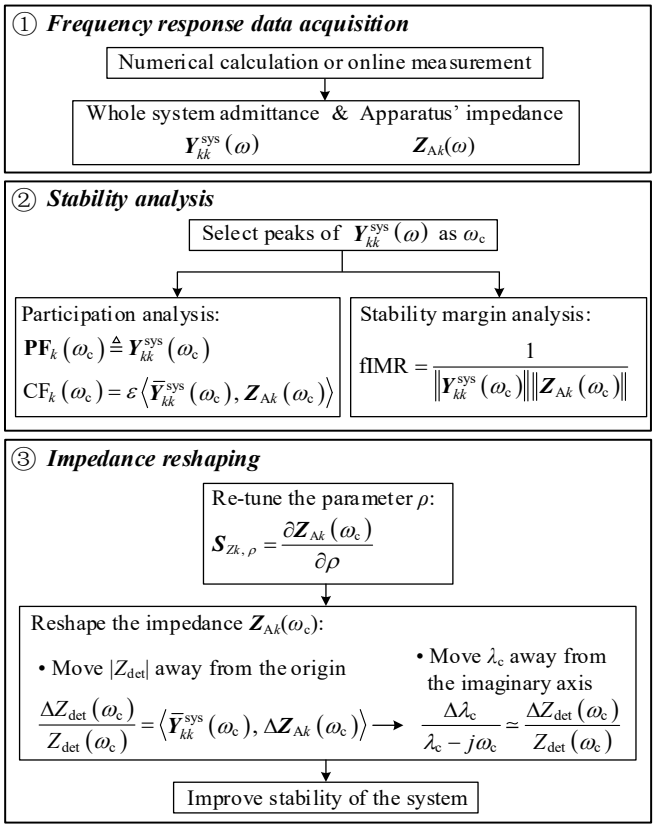

Fig. 4. The process of the fIMR based stability analysis method.

B. Comparison with NSC and GNSC

The well-known NSC is broadly applied in the frequency-spectra based stability analysis which focuses on the single apparatus at POI-*k*. The stability is determined using the Nyquist curve of the return ratio L_k as shown in (25), where Y_{gk} is the admittance of the grid and $Z_{\mathrm{ASISO}k}$ is the equivalent SISO admittances of the apparatus. Apparently, the sensitivity of L_k with respect to $Z_{\mathrm{ASISO}k}$ is Y_{gk}. However, return ratios L_k become different at different POIs without clarifying their correlation and easily produces inconsistent results. Therefore, unified sensitivity and stability margin analysis of the entire system for MIMO systems can hardly be built.

$$L_k(\omega) = Y_{gk}(\omega) Z_{\mathrm{ASISO}k}(\omega) \tag{25}$$

GNSC is for MIMO systems. The return ratio becomes a matrix $\boldsymbol{L}$ as shown in (26), where $\boldsymbol{Y}_{\mathrm{N}}$ is the admittance matrix of the network.

$$\boldsymbol{L}(\omega) = \boldsymbol{Y}_{\mathrm{N}}(\omega)\boldsymbol{Z}_{\mathrm{A}}(\omega) \tag{26}$$

The stability of the system can be determined with either the determinant of the return ratio matrix, L_{det}, or eigen values γ of the return ratio matrix. The sensitivity of L_{det} and the critical eigen value γ_{c} with respect to the elements of the impedance matrix can also be calculated to evaluate the stability margin of the entire system and guide the stability improvement. However, the calculation of L_{det} or γ requires full matrices of $\boldsymbol{Y}_{\mathrm{N}}$ and $\boldsymbol{Z}_{\mathrm{A}}$. Measuring the non-diagonal elements of $\boldsymbol{Y}_{\mathrm{N}}$ is practically difficult, as the focused POIs could be far from each other in MIMO systems.

Compared with NSC, the fIMR based method provides unified sensitivity with respect to Z_{det}, which endows it strong practical applicability for MIMO systems. Compared with and GNSC, as in (11), the proposed method merely requires the diagonal elements, which greatly decreases the difficulty of data acquisition. The features of the fIMR based method, NSC, and GNSC are illustrated in Fig. 5.

	fIMR	NSC	GNSC
Stability determination	Bode plots of Y^{sys}	Nyquist curves of Z_{SISO}	Nyquist curves of L_{det} or γ
Impedance Sensitivity	$\boldsymbol{Y}_{kk}^{\mathrm{sys}}(\omega)$	$Y_{gk}(\omega)$	$\frac{\partial L_{\mathrm{det}}(\omega)}{\partial Z_{\mathrm{A}ij}(\omega)}$ or $\frac{\partial \gamma(\omega)}{\partial Z_{\mathrm{A}ij}(\omega)}$
Stability margin	Unified	Not unified	Unified
Required elements	Diagonal elements	Diagonal elements	Full matrices

Fig. 5. Features comparison the fIMR based method, NSC, and GNSC.

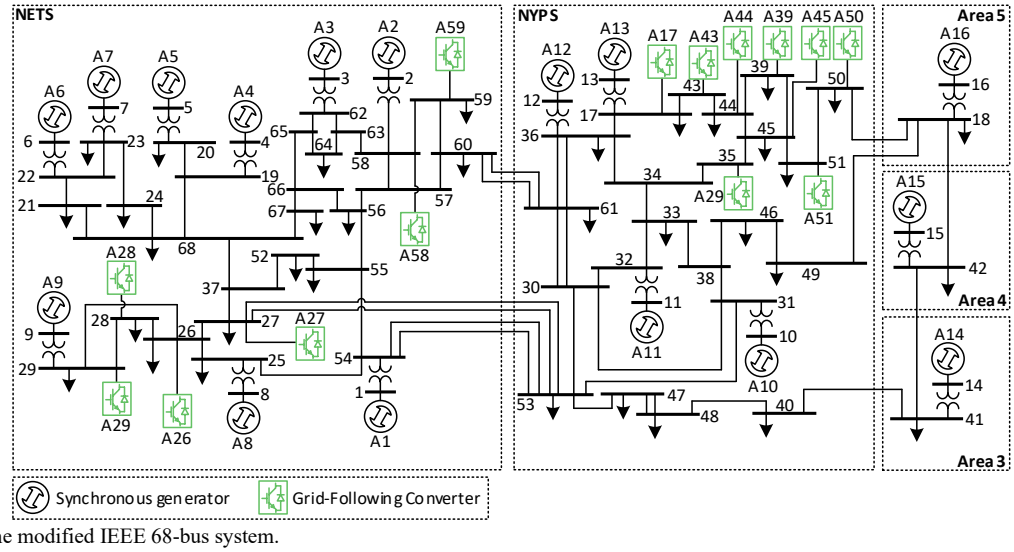

Fig. 6. Structure of the modified IEEE 68-bus system.

IV. Case Study

The modified IEEE 68-bus test system is adopted for validating the proposed method, as in Fig. 6. The controllers of IBRs are firstly detuned by different levels to represent a plain system with IBRs from multiple vendors and then are tuned with the proposed method. Only the bode plots calculated with the frequency-response-data are used through the entire analysis process. The detailed system data and the models can be found in [XX].

A. Stability Analysis

The whole-system admittances in the d-d frame of the POIs considering the connected IBRs are plotted in Fig. 7. Modes with frequencies of 26.1Hz, 30.4Hz, and 90.8Hz can be observed from peaks of the admittance curves. According to the participation factor defined in (12), a larger whole-system admittance indicates a higher participation level of the impedance of the apparatus. Thus, oscillation of 26.1Hz will be observed at POI-50 and POI-51; and oscillation of 30.4Hz and 90.8Hz will be observed at POI-26, POI-28, and POI-29.

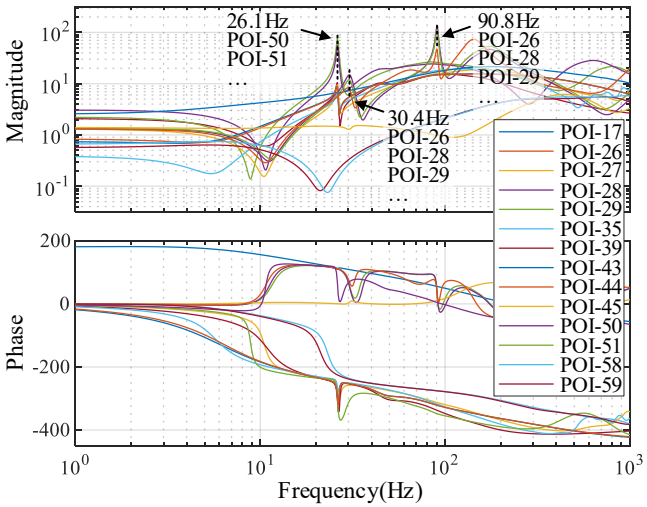

Fig. 7. Whole-system admittance at the POI with the IBR connected in the d-d frame.

The contribution factors, including the real and the imaginary parts, of IBRs are plotted in Fig. 8. According to the impedance-determinant-mode chain rule, the real part of the contribution factor represents the influence of apparatus that moves the determinant away from the zero point, which will influence the damping of modes. The imaginary part represents the influence on the frequency of the determinant. As an example, for 26.1Hz, it can be seen from Fig. 8 that the IBRs at POI-50 and POI-51 contribute more on the damping of modes. The positive real parts of the contribution factors indicate that scaling up the power rating of the IBRs at POI-50 and POI-51 will weaken the stability of the system at 26.1Hz. Similar analysis can be performed for 30.4Hz and 90.8Hz.

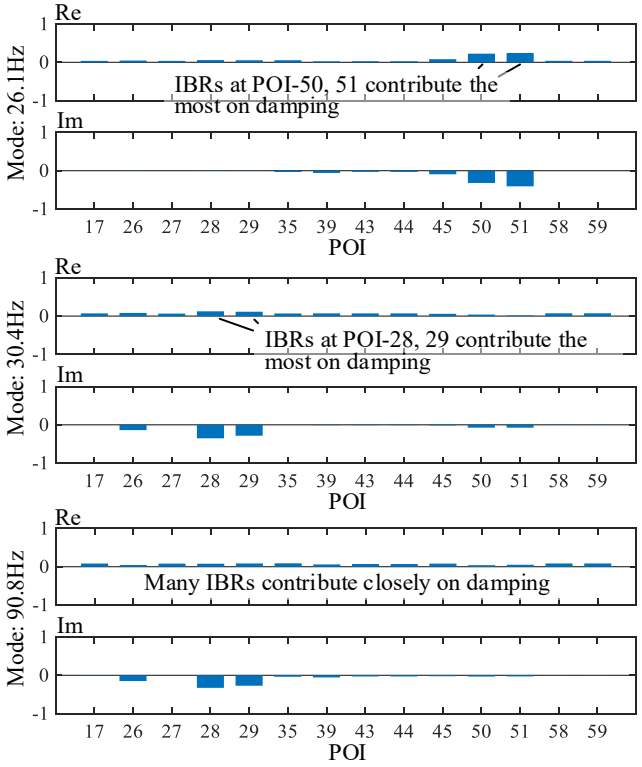

Fig. 8. Contribution factor of the IBRs.

The fIMR curves are shown in Fig. 9. From Fig. 9, fIMRs of POI-26, POI-28, POI-29 at 26.1Hz and 30.4Hz are very small, indicating deficit in stability margin at these POIs. Thus, the impedance reshaping should be conducted on POI-26, POI-28, POI-29 at 26.1Hz and 30.4Hz. The values of the whole-system admittance and the fIMR are summarized in TABLE I. $|Y_{kk}^{\text{sys-dd}}|$ represents magnitude of the whole-system admittance at POI-*k* in d-d frame.

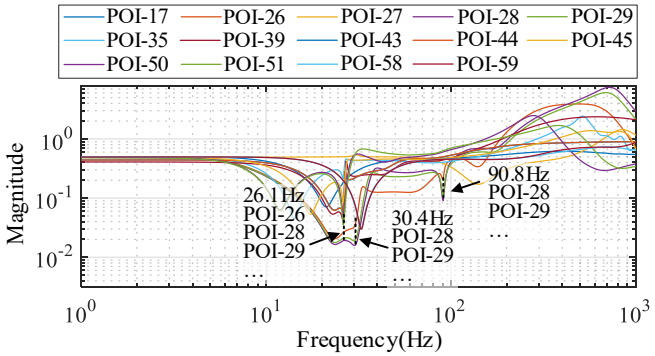

Fig. 9. fIMR at POIs with IBRs connected.

TABLE I
Values of the Whole-System Admittance and the fIMR

	ω_c: 26.1Hz		ω_c: 30.4Hz		ω_c: 90.8Hz	
	$\lvert Y_{kk}^{\text{sys-dd}}\rvert$	fIMR	$\lvert Y_{kk}^{\text{sys-dd}}\rvert$	fIMR	$\lvert Y_{kk}^{\text{sys-dd}}\rvert$	fIMR
POI-26	5.34	0.026	7.90	0.036	46.24	0.209
POI-28	6.58	0.019	14.95	0.016	135.0	0.091
POI-29	5.79	0.021	11.98	0.019	112.4	0.103
POI-50	55.09	0.044	8.00	0.544	24.01	0.603
POI-51	78.42	0.035	6.09	0.562	26.00	0.631

As shown in Fig. 10, fIMRs of POIs are illustrated by the heat map to show the distribution of the stability margin. If

multiple modes happen on one POI, the smallest fIMR is selected to represent the stability margin of this POI. The fIMRs of POI-26, -28, and -29 are smaller than 0.03pu. Thus, the IBRs at these POIs should be focused when reshaping the impedance.

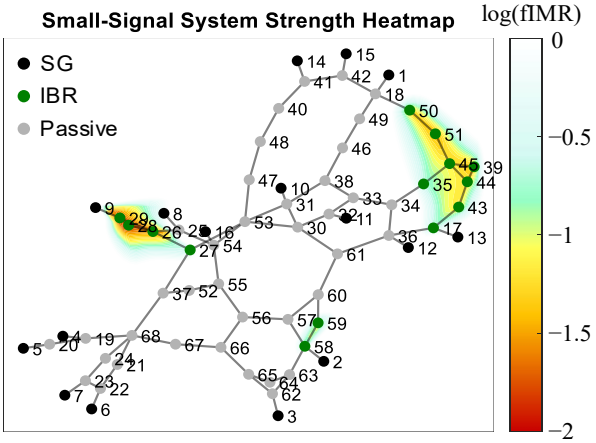

Fig. 10. fIMR heatmap of the system.

B. *Sensitivity Analysis and Impedance Reshaping*

Sensitivity analysis is conducted to guide the improving of the stability margin of the system at POIs whose damping ability is weak. As discussed in Section III, the impedance participation factor is identical to the whole-system admittance and the impedance-parameter sensitivity can be calculated with (18). According to the chain rule, the determinant-parameter sensitivity at POI-26, namely (19), can be shown in Fig. 11. From Fig. 11, increasing the parameter will enlarge the determinant's magnitude and thus enhance the system's stability, while the opposite holds true when it decreases. The determinant-parameter sensitivities of POI-28 and POI-29 are close to that of POI-26 as shown in Fig. 11.

Fig. 11 shows that increasing the filter inductor L, the current control bandwidth f_i, and the DC-link control bandwidth f_{dc} can all increase the magnitude of the determinant at 26.1Hz and 30.4Hz. By contrast, at 90.8Hz, increasing those parameters has less impact on the magnitude of the determinant but more impact on the frequency of the determinant. Similar results can be obtained from sensitivity analysis focused on POI-28 and POI-29. With the results shown by Fig. 11 and considering improving the stability margin at 26.1Hz and 30.4Hz is the target, the DC-link control bandwidth f_{dc} of the IBRs is increased from 400Hz to 600Hz.

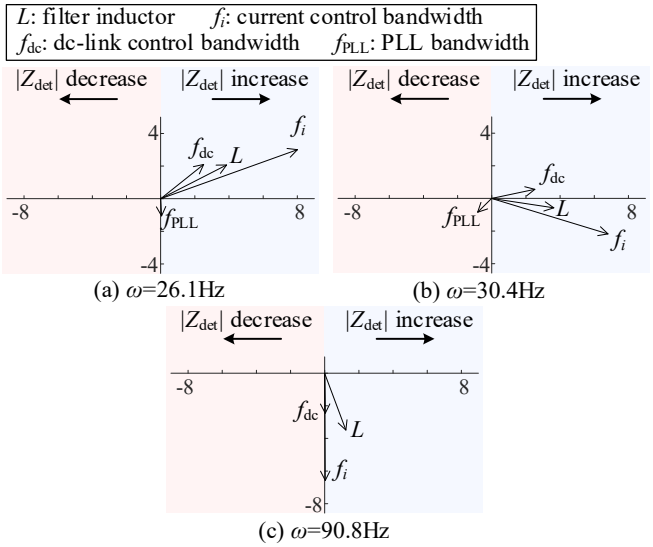

Fig. 11. The determinant-parameter sensitivity at POI-26 with the IBR connected after re-tuning the parameters.

The whole system admittance curves and the fIMR curves after tuning are plotted in Fig. 12 and Fig. 13, and are summarized in TABLE II. After tuning the parameters, the fIMR at the mode frequency 26.1Hz increases indicating increased stability margin. The mode with the frequency of 30.4Hz changes to a mode with the frequency of 42.9Hz and the whole-system admittance has smaller peaks, leading to a predictable suppression of the oscillation at POI-26, -28 and -29. fIMR at POI-26, -28 and -29 gain increments, indicating increased stability margin. The mode with frequency of 90.8Hz changes to the frequency of 109.1Hz, but the corresponding fIMR changes slightly meaning that the stability margin remains.

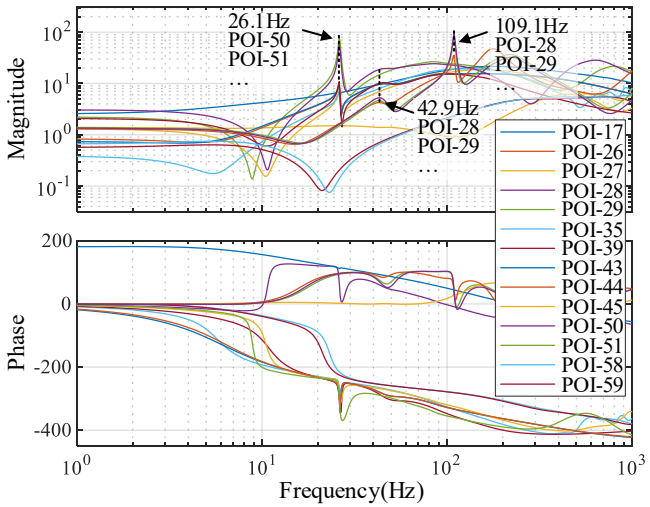

Fig. 12. Whole-system admittance at the POI with the IBR connected after retuning the parameters.

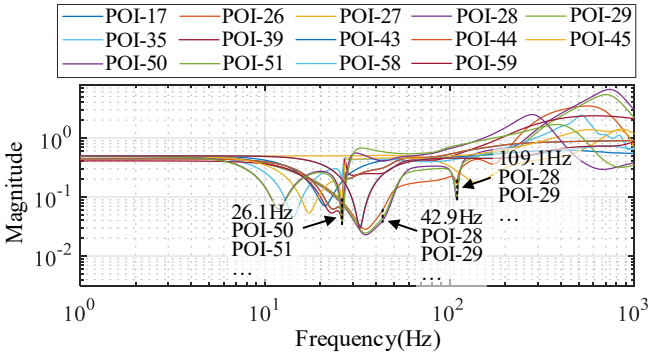

Fig. 13. fIMR at POIs with IBRs connected after re-tuning the parameters.

TABLE II
VALUES OF THE WHOLE-SYSTEM ADMITTANCE AND THE FIMR AFTER RETUNING

	ω_c: 26.1Hz		ω_c: 42.9Hz		ω_c: 109.1Hz	
	$\lvert Y_{kk}^{\text{sys-dd}}\rvert$	fIMR	$\lvert Y_{kk}^{\text{sys-dd}}\rvert$	fIMR	$\lvert Y_{kk}^{\text{sys-dd}}\rvert$	fIMR
POI-26	1.65	0.085	4.21	0.064	24.31	0.202
POI-28	1.60	0.076	5.22	0.042	70.81	0.115
POI-29	1.48	0.078	4.58	0.047	58.12	0.133
POI-50	56.88	0.043	19.12	0.407	22.56	0.712
POI-51	81.09	0.034	15.27	0.580	23.94	0.750

The heatmap after tuning is shown in Fig. 14. Comparing Fig. 14 with Fig. 10, the original red area around POI-26, POI-28, and POI-29 changes to yellow, representing that stability margins at them are improved. The result shows that the proposed fIMR based method can successfully identify the POIs with the deficit in stability margin and then guide the improvement.

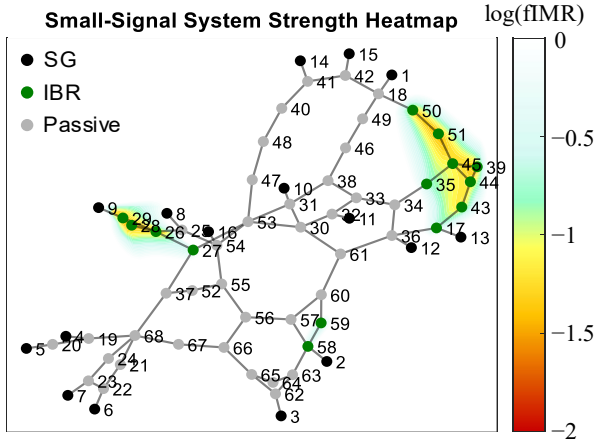

Fig. 14. fIMR heatmap of the system after parameter tuning.

We conduct time-domain simulation to further verify the proposed stability analysis method. The loads at POI-26, POI-28 and POI-29 are increased from 100% to 125% with a step of 25%. The waveforms and the FFT results are shown in Fig. 15. From Fig. 15, before tuning the parameters, oscillations at the frequencies of 30Hz and 91Hz can be observed. After parameter tuning, the oscillation at 30Hz can be suppressed, while the frequency of the other oscillation changes from 91Hz to 109Hz. The simulation results are consistent with the theoretical analysis shown in Figs. 11 and 14, thereby validating the effectiveness of the proposed method.

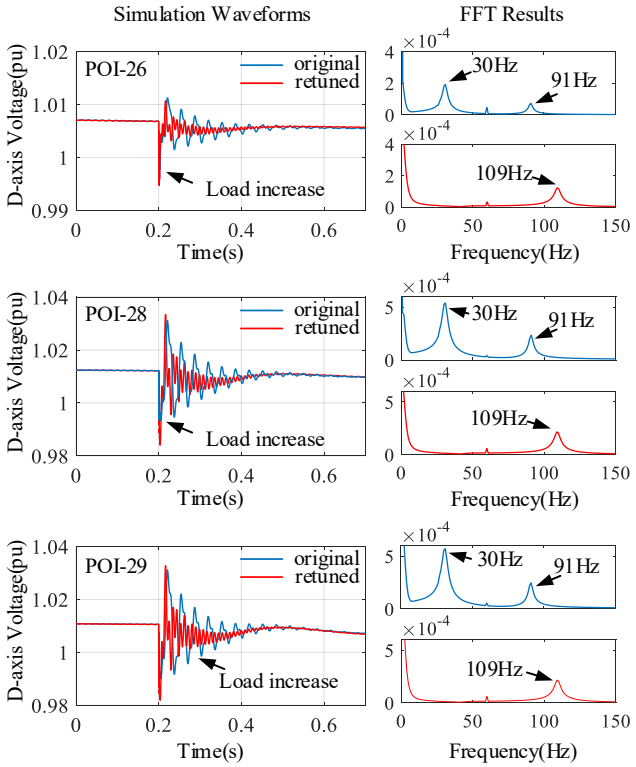

Fig. 15. Simulation results when the 25% step load increase is respectively added at POI-26, POI-28 and POI 29.

V. CONCLUSION

This paper introduces an fIMR method for stability margin analysis based on the impedance spectra. The fIMR method provides complete stability analysis at the frequency of the critical modes and provides a general indication of the stability margin through the frequency spectra. The entire process doesn't require the pole identification technology and possesses merits of convenience and intuitive interpretation. In the studied case, the fIMR successfully sorts out the weak points in the system and the determinant-impedance sensitivity is utilized as the guidance of the impedance reshaping to improve the stability of the critical mode. The fIMR method shows general merits over the NSC and the GNSC and is a more powerful and flexible method for the impedance-spectra based stability analysis.

REFERENCES

[1] IEA, "Global Energy Review 2025," Accessed: June. 20, 2025. [Online]. Available: https://www.iea.org/reports/global-energy-review-2025/electricity.
[2] Y. Gu and T. C. Green, "Power System Stability With a High Penetration of Inverter-Based Resources," *Proceedings of the IEEE*, vol. 111, no. 7, pp. 832–853, Jul. 2023.
[3] Y. Cheng *et al.*, "Real-World Subsynchronous Oscillation Events in Power Grids With High Penetrations of Inverter-Based Resources," *IEEE Transactions on Power Systems*, vol. 38, no. 1, pp. 316–330, Jan. 2023.
[4] J. Sun, 'Impedance-Based Stability Criterion for Grid-Connected Inverters', *IEEE Transactions on Power Electronics*, vol. 26, no. 11, pp. 3075–3078, Nov. 2011.
[5] L. Fan and Z. Miao, 'Admittance-Based Stability Analysis: Bode Plots, Nyquist Diagrams or Eigenvalue Analysis?', *IEEE Transactions on Power Systems*, vol. 35, no. 4, pp. 3312–3315, Jul. 2020.

[6] Q. Chen, S. Bu, and C. Y. Chung, "Small-Signal Stability Criteria in Power Electronics-Dominated Power Systems: A Comparative Review," *Journal of Modern Power Systems and Clean Energy*, vol. 12, no. 4, pp. 1003–1018, Jul. 2024.

[7] Q. Chen and S. Bu, "Impedance-Based Stability Analysis of Power System Wideband Oscillations: A Bridge between s Domain and Frequency Domain," *IEEE Transactions on Power Systems*, vol. 39, no. 4, pp. 5854–5868, Jul. 2024.

[8] W. Xu, Z. Huang, Y. Cui, and H. Wang, 'Harmonic resonance mode analysis', *IEEE Transactions on Power Delivery*, vol. 20, no. 2, pp. 1182–1190, Apr. 2005.

[9] Y. Zhan, X. Xie, H. Liu, H. Liu, and Y. Li, "Frequency-Domain Modal Analysis of the Oscillatory Stability of Power Systems With High-Penetration Renewables," *IEEE Transactions on Sustainable Energy*, vol. 10, no. 3, pp. 1534–1543, Jul. 2019.

[10] Y. Zhan, X. Xie, and Y. Wang, "Impedance Network Model Based Modal Observability and Controllability Analysis for Renewable Integrated Power Systems," *IEEE Transactions on Power Delivery*, vol. 36, no. 4, pp. 2025–2034, Aug. 2021.

[11] Y. Gu, Y. Li, Y. Zhu, and T. C. Green, "Impedance-Based Whole-System Modeling for a Composite Grid via Embedding of Frame Dynamics," *IEEE Transactions on Power Systems*, vol. 36, no. 1, pp. 336–345, Jan. 2021.

[12] Y. Zhu, Y. Gu, Y. Li, and T. C. Green, 'Participation Analysis in Impedance Models: The Grey-Box Approach for Power System Stability', *IEEE Transactions on Power Systems*, vol. 37, no. 1, pp. 343–353, Jan. 2022.

[13] Y. Zhu, Y. Gu, Y. Li, and T. C. Green, "Impedance-Based Root-Cause Analysis: Comparative Study of Impedance Models and Calculation of Eigenvalue Sensitivity," *IEEE Transactions on Power Systems*, vol. 38, no. 2, pp. 1642–1654, Mar. 2023.

[14] Y. Zhu, T. C. Green, X. Zhou, Y. Li, D. Kong, and Y. Gu, "Impedance Margin Ratio: a New Metric for Small-Signal System Strength," *IEEE Transactions on Power Systems*, vol. 39, no. 6, pp. 7291-7303, Nov. 2024.

[15] Y. Liao, H. Wu, X. Wang, M. Ndreko, R. Dimitrovski, and W. Winter, "Stability and Sensitivity Analysis of Multi-Vendor, Multi-Terminal HVDC Systems," *IEEE Open Journal of Power Electronics*, vol. 4, pp. 52–66, 2023.

[16] H. Wu and X. Wang, "Dynamic Impact of Zero-Sequence Circulating Current on Modular Multilevel Converters: Complex-Valued AC Impedance Modeling and Analysis," *IEEE Journal of Emerging and Selected Topics in Power Electronics*, vol. 8, no. 2, pp. 1947–1963, Jun. 2020.

[17] Z. Xu *et al.*, "A Complete HSS-Based Impedance Model of MMC Considering Grid Impedance Coupling," *IEEE Trans. Power Electron.*, vol. 35, no. 12, pp. 12929–12948, Dec. 2020.

[18] L. Orellana, L. Sainz, E. Prieto-Araujo, and O. Gomis-Bellmunt, "Stability Assessment for Multi-Infeed Grid-Connected VSCs Modeled in the Admittance Matrix Form," *IEEE Transactions on Circuits and Systems I: Regular Papers*, vol. 68, no. 9, pp. 3758–3771, Sep. 2021.

[19] D. Yang and Y. Sun, "SISO Impedance-Based Stability Analysis for System-Level Small-Signal Stability Assessment of Large-Scale Power Electronics-Dominated Power Systems," *IEEE Transactions on Sustainable Energy*, vol. 13, no. 1, pp. 537–550, Jan. 2022.

[20] H. Zhang, M. Saeedifard, X. Wang, Y. Meng, and X. Wang, "System Harmonic Stability Analysis of Grid-Tied Interlinking Converters Operating Under AC Voltage Control Mode," *IEEE Transactions on Power Systems*, vol. 37, no. 5, pp. 4106–4109, Sep. 2022.

[21] S. Jiang, Y. Zhu, and G. Konstantinou, "Settling Angle-Based Stability Criterion for Power-Electronics-Dominated Power Systems," *IEEE Transactions on Power Electronics*, vol. 38, no. 3, pp. 2972–2984, Mar. 2023.

[22] Y. Tan, Y. Sun, J. Lin, L. Yuan, and M. Su, "Revisit Impedance-Based Stability Analysis of VSC-HVDC System," *IEEE Transactions on Power Systems*, vol. 39, no. 1, pp. 1728–1738, Jan. 2024.

[23] Y. Liao, X. Wang, and X. Wang, "Frequency-Domain Participation Analysis for Electronic Power Systems," *IEEE Transactions on Power Electronics*, vol. 37, no. 3, pp. 2531–2537, Mar. 2022.

[24] H. Xu, D. Gan, Q. Zhang, W. Huang, P. Zeng, and R. Huang, "A Small-Signal Stability Analysis Method Based on Minimum Characteristic Locus and Its Application in Controller Parameter Tuning," *IEEE Transactions on Power Systems*, vol. 39, no. 2, pp. 3798–3810, Mar. 2024.

[25] A. Alassaf and L. Fan, "Randomized Dynamic Mode Decomposition for Oscillation Modal Analysis," *IEEE Transactions on Power Systems*, vol. 36, no. 2, pp. 1399–1408, Mar. 2021.

[26] L. Fan, Z. Miao, P. Koralewicz, S. Shah, and V. Gevorgian, "Identifying DQ-Domain Admittance Models of a 2.3-MVA Commercial Grid-Following Inverter via Frequency-Domain and Time-Domain Data," *IEEE Transactions on Energy Conversion*, vol. 36, no. 3, pp. 2463–2472, Sep. 2021.

[27] R. Schumacher, G. H. C. Oliveira, and L. F. M. Rodrigues, "Enhancing rational approximation of wideband resonant MIMO systems with frequency-domain data," *European Journal of Control*, vol. 78, p. 101000, Jul. 2024.

[28] Y. Liao *et al.*, "Neural Network Design for Impedance Modeling of Power Electronic Systems Based on Latent Features," *IEEE Transactions on Neural Networks and Learning Systems*, vol. 35, no. 5, pp. 5968–5980, May 2024.

[29] W. Wang, X. Shi, G. Wu, and Y. Cao, "Interaction Between Grid-Forming Converters With AC Grids and Damping Improvement Based on Loop Shaping," *IEEE Transactions on Power Systems*, vol. 39, no. 1, pp. 1905–1917, Jan. 2024.

[30] H. Li, B. Hu, H. Nian, Y. Liao, L. Xiong, and Z. Liang, "Impedance Characteristic Analysis and Phase-Locked Angle Feedforward-Based Stability Improvement for LCC-HVDC in Sending AC Grid," *IEEE Transactions on Sustainable Energy*, vol. 16, no. 1, pp. 588–600, Jan. 2025.